ChemCatChem

Research Article
doi.org/10.1002/cctc.202400502

Chemistry Europe
European Chemical Societies Publishing

www.chemcatchem.org

Direct Z-Scheme Heterostructure of Nanoparticle-CdSe on Nanorod-$NaNbO_3$: Facile Hydro-thermal Construction and Superior Photocatalytic Activity and Stability in H_2 Evolution

Linlin Gao,[a] Shengyuan Chang,[a] Huajun Gu,[a] Huihui Zhang,[a] Yamei Huang,[a] Xinglin Wang,[a] Qin Li,[a] and Wei-Lin Dai*[a]

The advancement of exceptionally effective catalysts that are photostable is significantly important for the sustainable conversion of solar energy into hydrogen. Combining the strengths of $NaNbO_3$ and CdSe in a fabricated heterojunction has been pursued in photocatalysis to enhance the performance while addressing CdSe's stability. In this study, nanoparticle-CdSe was deposited on $NaNbO_3$ nanorods via hydrothermal method, and the optimal composite ratio of CdSe/$NaNbO_3$ heterojunction achieved a photocatalytic hydrogen production of 2510 $\mu mol\,g^{-1}h^{-1}$. The enhancement is ascribed to the formation of a Z-scheme heterojunction by the interface contact between CdSe and $NaNbO_3$.The migration of electrons from $NaNbO_3$ to CdSe was revealed by charge density difference results in DFT calculation. Work function of samples demonstrated the equilibrium of Fermi level and a corresponding shift of the band structure in the heterojunction. The H adsorption free energy (ΔG_{H^*}) for the heterojunction was 0.26 eV, suggesting a reduced energy barrier for hydrogen generation. Notably, the stable structure of $NaNbO_3$ endows the composites with excellent chemical stability, maintaining more than 80% activity after six hydrogen production cyclic tests. This work offers valuable insights into the development of direct Z-scheme structure catalysts for photocatalytic water splitting.

Introduction

The quest for sustainable energy, known for its environmentally friendly nature and long-term viability, has received widespread endorsement as a strategy to realize sustainable development and advance environmental conservation efforts. Photocatalytic hydrogen production via semiconductor catalysts represents an effective approach for converting solar energy into hydrogen energy. The advancement of semiconductor photocatalytic technology has unveiled a spectrum of semiconductors, including g-C_3N_4,[1,2] TiO_2,[3,4] ZnO,[5–8] GDY,[9,10] In_2O_3,[11] and CdS,[12–14] which demonstrate excellent performance in photocatalysis. Perovskite materials are held in high regard as promising photocatalysts owing to their structurally stable nature and favorable dielectric properties.[4–6]

Niobate is a prevalent wide bandgap semiconductor material, categorized into alkali metal niobate, cation-deficient alkaline earth niobate MNb_2O_{15} (M=Cu, Mg, Co, Ca, Ni, Zn), and M_5NbO_{15} (M=Ba, Sr) based on its properties.[15] In the crystal structure, Nb tends to form a hexacoordinated [NbO_6] octahedron through coordination, serving as a structural unit to create various niobate materials by adjusting co-apical angles and co-prisms. Notably, the octahedral units [NbO_6] in sodium niobate ($NaNbO_3$) facilitate efficient charge migration within its crystal lattice.[16,17] Exhibiting exceptional stability and dependable catalytic reactivity within the ultraviolet spectrum, $NaNbO_3$ is widely favored in the realm of photocatalysis.[18–20] Nonetheless, the wide bandgap of $NaNbO_3$ leads to pronounced recombination of photogenerated carriers, thereby constraining its applicability within the visible light range.[21–23]

To enhance the catalytic efficacy of materials further, strategies such as elemental doping, defect engineering, and composite heterojunction design can be employed.[24–27] The fabrication of composite heterojunctions enables the segregation of electrons and holes onto distinct materials through interfacial interactions, presenting an optimal solution to mitigate photogenerated carrier recombination and elevate photocatalytic performance.[8,24,25] Within the wide spectrum of semiconductor photocatalysts, CdSe has garnered interest owing to its appropriate bandgap and pronounced absorption in the visible spectrum.[28–30] However, the stability of CdSe requires enhancement owing to its susceptibility to photocorrosion. Consequently, the incorporation of highly stable $NaNbO_3$ as a matrix can bolster the stability of the composite while leveraging CdSe to augment light-absorbing properties and modulate the band structure of the composites, thereby amplifying the hydrogen production activity and stability of the resulting composite materials, which holding significant exploratory implications.[31,32]

In this work, the synergistic integration of the stability characteristics of $NaNbO_3$ and the robust light-responsive properties of CdSe was leveraged to fabricate a Z-scheme

[a] L. Gao, S. Chang, H. Gu, H. Zhang, Y. Huang, X. Wang, Q. Li, W.-L. Dai
Department of Chemistry and Shanghai Key Laboratory of Molecular Catalysis and Innovative Materials
Fudan University
Shanghai 200433, P. R. China
E-mail: wldai@fudan.edu.cn

Supporting information for this article is available on the WWW under https://doi.org/10.1002/cctc.202400502

heterojunction photocatalyst for the purpose of hydrogen generation through water splitting. Sodium niobate nanorods were prepared through hydrothermal and calcination processes, followed by the deposition of CdSe nanoparticles (NPs) onto the pre-synthesized $NaNbO_3$ through a hydrothermal process. The composite demonstrated remarkable photocatalytic hydrogen production activity, achieving a performance of 2510 $\mu mol\,g^{-1}\ h^{-1}$, and maintaining a retention rate of over 80% even after six cycles. Characterization methodologies and theoretical computations corroborated the successful fabrication of the CdSe/$NaNbO_3$ heterojunction, elucidating the Z-scheme reaction mechanism governing the migration of electrons from $NaNbO_3$ to CdSe.

Results and Discussion

Preparation and characterization of CdSe/$NaNbO_3$

The synthetic procedure for the CdSe/$NaNbO_3$ heterostructure is illustrated in Scheme 1. Initially, $NaNbO_3$ nanorods were synthesized via a hydrothermal process at a temperature of 180 °C, subsequent to which calcination was conducted at a temperature of 500 °C, employing niobium pentoxide and NaOH as primary precursors. Then, the resultant product was mixed with $CdCl_2 \cdot 2.5H_2O$, Se powder, DETA, and $N_2H_4 \cdot H_2O$, then the CdSe/$NaNbO_3$ heterojunctions were fabricated through a hydrothermal approach, facilitating the in-situ growth of CdSe NPs on the surface of $NaNbO_3$.

The morphology of the prepared compounds is clearly elucidated via transmission electron microscopy (TEM) images. In Figure 1a, the $NaNbO_3$ material exhibits a typical smooth nanorod structure with dimensions ranging from 100 to 600 nm, thereby providing a stable platform for the sequential loading of CdSe. The synthesized CdSe (Figure 1b & 1c) appears as NPs or short nanorods, displaying a size range of 2 to 10 nm. TEM images (Figure 1d & 1e) demonstrate that agglomeration of CdSe NPs occurs, resulting in the formation of spheroids prior to their surface loading onto $NaNbO_3$ nanorods. Detailed microstructural information is unveiled in high-resolution TEM (HRTEM) images of the CdSe/$NaNbO_3$ composite (Figure 1f), showcasing the lattice fringes of both materials. The lattice spacing of 0.39 nm corresponds to the (101) planes of $NaNbO_3$,

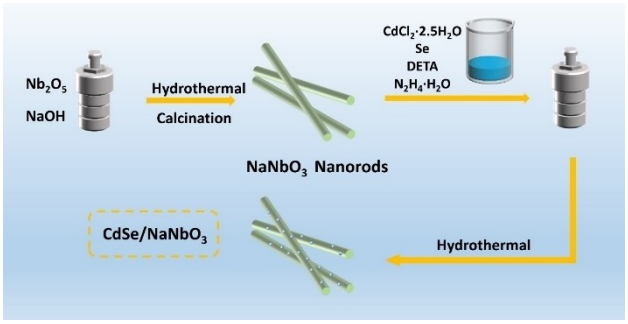

Scheme 1. Illustration of the preparation of CdSe/$NaNbO_3$.

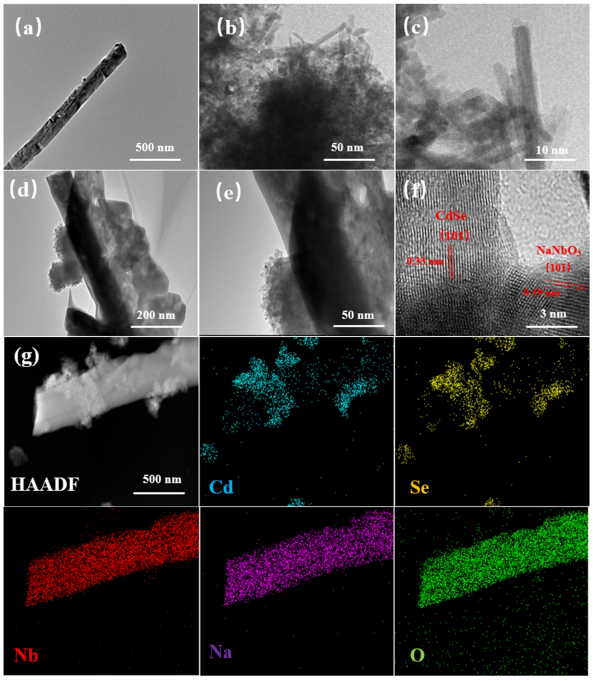

Figure 1. (a) TEM images of $NaNbO_3$ nanorod. (b,c) TEM images of CdSe. (d-f) TEM images of CdSe/$NaNbO_3$. (g) Elemental mapping images of CdSe/$NaNbO_3$ composite.

while the lattice spacing of 0.33 nm corresponds to the (101) planes of CdSe. Furthermore, the elemental distribution within CdSe/$NaNbO_3$ is validated through EDS analysis (Figure 1 g), highlighting the surface dispersion of Cd and Se elements, with Na, Nb, and O elements primarily concentrated in the middle region, exhibiting a distinct rod-like pattern.

Employing X-ray diffraction (XRD) analysis, the diffraction structures of CdSe, $NaNbO_3$, and their composite were characterized, as depicted in Figure 2a. Distinct diffraction peaks were observed in the XRD pattern of CdSe at 23.9°, 25.4°, 27.1°, 35.1°, 42°, 46°, and 49.7°, corresponding to the (100), (002), (101), (102), (110), (103), and (112) planes of CdSe.[32–34] Similarly, the diffraction peaks of $NaNbO_3$ appeared at 22.9°, 32.6°, 46.5°, 52.6°, 58.1°, and 68.1°, correlating to the (001), (110), (002), (021), (112), and (022) planes of $NaNbO_3$,[12] indicating the successful preparation of both materials. Furthermore, the XRD structure of the composites at different ratios is presented in Figure 2b, where the diffraction peaks of $NaNbO_3$ are clearly visible in all composites. However, the intensity of peaks observed in CdSe was comparatively weak, a phenomenon that could be ascribed to the low concentration of CdSe present in the heterojunction and its propensity to cluster. On the contrary, with an increase in the quantity of CdSe content, the intensity of peaks gradually escalated, evincing the presence of a positive correlation linking the amount of CdSe present to the intensity of peaks. The survey spectrum of XPS depicted in Figure 2c reveals the presence of Nb, Se, and Cd elements, providing clear evidence of the successful preparation of the material. Figure 2d depicts the XPS spectrum of Nb 3d. The Nb $3d_{5/2}$ and Nb $3d_{3/2}$ main peaks are evident at binding energies

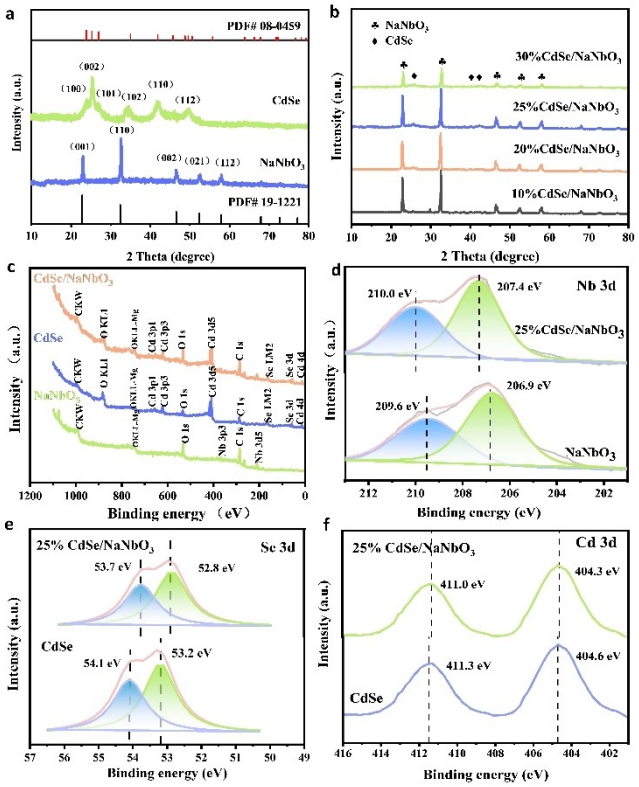

Figure 2. (a) XRD of CdSe and $NaNbO_3$. (b) XRD of CdSe/$NaNbO_3$. Heterojunction. (c) XPS survey spectrum of pristine CdSe, $NaNbO_3$ and CdSe/$NaNbO_3$ heterojunction photocatalyst. (d) XPS spectra of Nb 3d for pristine $NaNbO_3$ and CdSe/$NaNbO_3$ heterojunction. (e, f) XPS spectra of Se 3d and Cd 3d for pristine CdSe and CdSe/$NaNbO_3$ heterojunction.

of 206.9 and 209.6 eV, indicating the presence of the Nb element in the Nb^{5+} within the $NaNbO_3$ compound.[35] Notably, a positive shift in binding energy is discernible for the Nb 3d peaks, with values of 207.4 and 210.0 eV, correlating to Nb $3d_{5/2}$ and Nb $3d_{3/2}$. Furthermore, Figure 2e and 2f present the XPS spectra for Se 3d and Cd 3d. In the Se spectrum, distinct peaks at 53.2 and 54.1 eV are observed, signifying the presence of Se $3d_{5/2}$ and Se $3d_{3/2}$ states in CdSe, respectively. In the case of composite materials, these peaks shift to lower binding energy, specifically at 52.8 and 53.7 eV. This shift suggests that the Se species in the composites experience a reduced binding energy compared to pure CdSe.[36] Regarding the Cd 3d orbital, CdSe exhibits characteristic peaks at 404.6 eV (Cd $3d_{5/2}$) and 411.3 eV (Cd $3d_{3/2}$). Upon the formation of CdSe/$NaNbO_3$ composites, these peaks undergo a slight shift towards lower binding energy (404.3 and 411.0 eV). Importantly, the significant binding energy shift observed in the XPS peaks provides evidence for the successful preparation of the heterojunction and the migration of electrons in it. In short, the Cd 3d and Se 3d peaks both shift towards lower binding energies, while the Nb 3d peaks shift towards higher binding energies in the CdSe/$NaNbO_3$ heterojunction. These results suggest a strong interfacial synergy among the two substances, effectively facilitating electron transport from $NaNbO_3$ to CdSe, signifying the establishment of a favorable charge distribution within the heterojunction.

Photocatalytic hydrogen evolution activity

In this study, Na_2S and Na_2SO_3 were used as sacrificial agents for hydrogen production, with a catalyst dosage of 20 mg. Additionally, 1 %Pt was added as a co-catalyst during the photocatalytic process for water splitting. This experiment is conducted within the visible light range with a filter of UV and IR light. Circulating cooling water and a fan were used to dissipate heat generated by the Xe lamp. As shown in Figure 3a, the photocatalytic activities of CdSe and $NaNbO_3$ were 1120 $\mu mol\,g^{-1}h^{-1}$ and 445 $\mu mol\,g^{-1}h^{-1}$, respectively. The catalytic performance of the composite materials exhibited an initial rise followed by a decline corresponding to the augmentation of CdSe content. At a CdSe concentration of 25 %, the composite catalyst demonstrated its peak activity at 2510 $\mu mol\,g^{-1}h^{-1}$, surpassing that of pure $NaNbO_3$ and CdSe by 5.6 and 2.2 times, respectively. The comparative results of the documented performance of several photocatalysts based on $NaNbO_3$ are illustrated in Table 1.

This finding indicates that the composite catalyst effectively enhances the photocatalytic performance. The activity of composite materials improves with the increase of CdSe loading. However, excessive CdSe loading may coat the surface of $NaNbO_3$, inhibiting carrier excitation and introducing excess carrier recombination sites, leading to reduced activity. The improved hydrogen production activity of the composite catalyst confirms the efficacy of heterojunction construction in enhancing photocatalytic performance compared to related studies.

To further assess the catalytic efficacy of the heterojunction, we conducted an analysis of the apparent quantum efficiency (AQE) for the 25 % CdSe/$NaNbO_3$ composition, which demon-

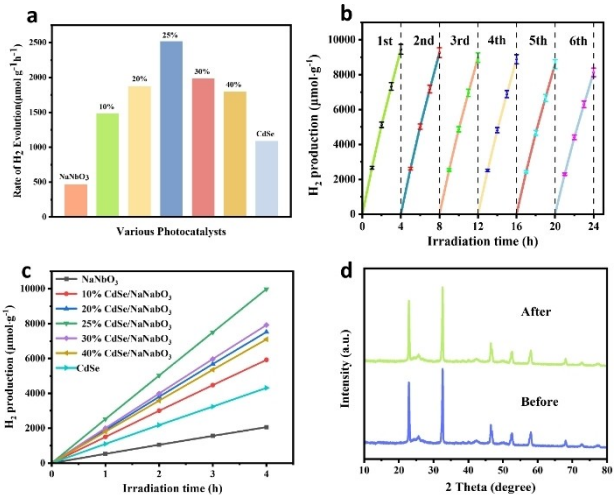

Figure 3. (a, b) Hydrogen production performance of CdSe/$NaNbO_3$ composite catalysts with different ratios. (c) Cyclic test of photocatalytic hydrogen production. (d) XRD pattern of catalysts before and after cycle hydrogen production.

Table 1. Comparison of the reported activity of some $NaNbO_3$-based photocatalysts.

Photocatalyst	Light source	Incident light (nm)	Sacrificial agents	Mass of catalyst (mg)	H_2 (μmol /h)	Ref.
CdSe/$NaNbO_3$	**300 W Xe**	**>300**	**Na_2S/Na_2SO_3 (0.35 M/0.25 M)**	**20**	**50**	**This work**
Cubic $NaNbO_3$ nanowires	300 W Xe	>300	Methanol (20% vol)	100	70	[37]
$(LaCo)_{0.03}(NaNb)_{0.97}O_3$	300 W Xe	>400	Methanol (20% vol)	300	11.9	[38]
$In_2O_3/NaNbO_3$ Rods	300 W Xe	>300	Methanol (20% vol)	300	13	[39]
Pt/N-rGO/N-$NaNbO_3$	300 W Xe	>300	Methanol (20% vol)	100	6	[12]
CuS/$NaNbO_3$	300 W Xe	>320	Na_2S/Na_2SO_3 (0.35 M/0.25 M)	20	39	[40]

strated the highest hydrogen production activity at a specific incident wavelength under identical reaction conditions. The resulting AQE calculations are detailed in Table 2.

Given that $NaNbO_3$ constitutes the primary component of the composite, it exhibits notable quantum efficiency in the ultraviolet spectrum, reaching 2.5% at 320 nm before gradually declining and stabilizing with increasing wavelengths. Furthermore, we evaluated the stability of the 25% CdSe/$NaNbO_3$ composite catalyst (Figure 3c), which displayed slight activity decay over six cycles, retaining over 80% of its initial activity. Concurrently, the XRD patterns of the catalyst pre- and post-reaction are depicted in Figure 3d. It is evident that the material's characteristic diffraction peak positions and intensities remained largely unchanged before and after the reaction, indicating the material's capacity to maintain structural and operational stability.

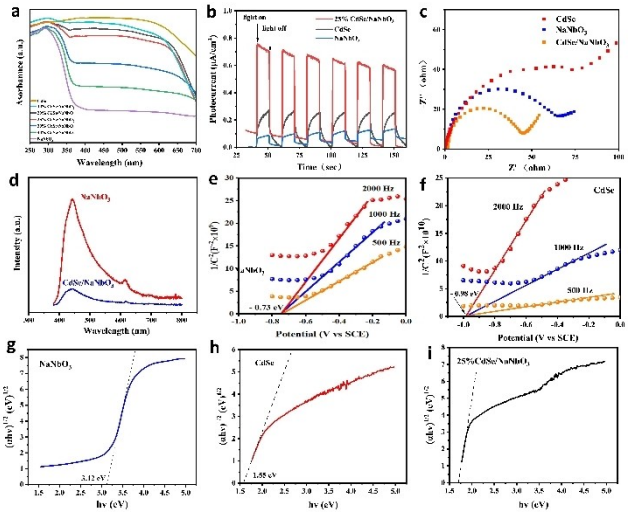

Figure 4. (a) UV – vis diffuse reflectance spectra (DRS) of pure CdSe, $NaNbO_3$, and CdSe/$NaNbO_3$ heterostructures. (b) Photocurrent spectra and (c) EIS plots of pure CdSe, $NaNbO_3$, and CdSe/$NaNbO_3$. (d) Time-resolved PL spectrum of pure $NaNbO_3$ and CdSe/$NaNbO_3$. (e,f) Mott – Schottky plots of pure CdSe and $NaNbO_3$. (g-i) Tauc plots of $NaNbO_3$, CdSe and CdSe/$NaNbO_3$.

Photoelectrochemical property characterization and photocatalytic mechanism

Figure 4a displays the UV-vis DRS for the diverse compositions of the samples. The results indicate that all specimens manifest wide absorption spectrum, with $NaNbO_3$ nanorods displaying a pronounced absorption edge in the UV region. This finding is in agreement with the migration of electrons from the O 2p orbital to the Nb 4d orbital within $NaNbO_3$. CdSe demonstrates strong photo absorption across the entire wavelength spectrum, with no reduction in absorption intensity until surpassing 550 nm. This underscores their remarkable capacity to harness incident light within the ultraviolet and visible ranges. $NaNbO_3$ exhibits good absorption in the wavelength less than 350 nm, indicating its excellent photocatalytic performance in the ultraviolet range. As for the visible light range, the light absorption of $NaNbO_3$ is significantly reduced, but as the CdSe content increases, the light absorption performance of the heterojunction in the visible light region gradually improves. Furthermore, the band gaps of the different materials were determined via the Kubelka–Munk method, the corresponding Tauc curve can be obtained through parameter transformation, and the material's band gap can be approximated by its intersection point with the abscissa axis. As depicted in Figure 4 g; h & i, it is evident that the band gaps of $NaNbO_3$, CdSe, and 25% CdSe/$NaNbO_3$ are 3.12 eV, 1.55 eV, and 1.72 eV, respectively. The composite materials exhibit a band gap that falls within the range delineated by the two individual pure constituents, showcasing a considerable decrease in value when contrasted with the band gap of $NaNbO_3$. This reduction pointed out that CdSe loading is able to effectually adjust the original band gap structure and enable the composites to utilize light in a broader range and generate more carriers to participate in the reaction.

Table 2. Apparent quantum efficiency (AQE) of CdSe/$NaNbO_3$.

Wavelength (nm)	320	350	400	420
AQE (%)	2.5	1.5	1.3	1.2

Photocurrent serves as a pivotal characterization technique for examining the optical responsiveness and photogenerated carrier migration capabilities of composite materials. Photocurrent assessments were illustrated in Figure 4b. The findings reveal a notably heightened photocurrent intensity of the composite materials, underscoring the superior light responsiveness and carrier migration capacity of the CdSe/$NaNbO_3$ composite. This attribute is poised to facilitate electron transfer at the interfacial regions during the reaction. The electrochemical impedance spectroscopy (EIS) technique enables the assessment of impedance, serving as a crucial indicator for evaluating carrier transport and recombination within catalyst materials. In this study, the electrical impedance of CdSe, $NaNbO_3$, and their composites was measured, with the corresponding results presented in Figure 4c. Notably, the electrical impedance radius of the composites exhibited a substantial reduction compared to that of the individual materials. This observation signifies that the integration of these materials can effectively mitigate carrier transport resistance, thereby facilitating enhanced efficiency in carrier migration and transport, ultimately leading to improved reaction performance. Under 360 nm, the PL test outcomes for both $NaNbO_3$ and the 25% CdSe/$NaNbO_3$ composite are depicted in Figure 4d. There is no obvious excitation of CdSe under the wavelength of 360 nm. The PL peak intensity of $NaNbO_3$ surpasses that of the composites significantly, implying that the incorporation of CdSe onto $NaNbO_3$ serves to effectively inhibit the electron-hole recombination. The positive gradients exhibited by both substances implied n-type semiconductor characteristics during Mott-Schottky (M–S) electrochemical assessments. Flat-band potentials of $NaNbO_3$ and CdSe were measured as −0.73 eV and −0.98 eV, respectively. Typically, there exists a differential of 0.24 V between a standard hydrogen electrode (SHE) and a saturated calomel electrode (SCE). The flat band potential is situated near the conduction band (CB) position (approximately −0.10 to −0.2 V) for n-type semiconductors.[41–44] Consequently, the conduction band (CB) positions of $NaNbO_3$ and CdSe were determined as −0.59 eV and −0.84 eV, respectively.

In order to enhance the verification of the material structure and reaction mechanism, theoretical calculations were conducted. Vienna Ab initio Simulation Package (VASP)[45] was used in the first principle calculations, employing the projector augmented wave (PAW) method.[46] The exchange functional is implemented utilizing the Perdew-Burke-Ernzerhof (PBE)[45] functional in conjunction with the DFT–D correction.[47] A plane-wave basis cut-off energy of 450 eV is employed. Brillouin zone integration is conducted to optimize both geometry and lattice size, using a 3*2*1 Monkhorst-Pack k-point sampling scheme.[48] A convergence energy threshold of 10^{-5} eV was utilized in self-consistent calculations. Equilibrium geometries and lattice constants are optimized with a maximum stress on each atom within 0.02 eV/Å. Figure 5a depicts the schematic structure model of CdSe/$NaNbO_3$. As shown in Figure 5b, the charge density difference analysis of the composite reveals a predominant electron depletion region within the $NaNbO_3$, while the electron accumulation region is primarily concentrated in the CdSe region. These findings suggest a potential migration of

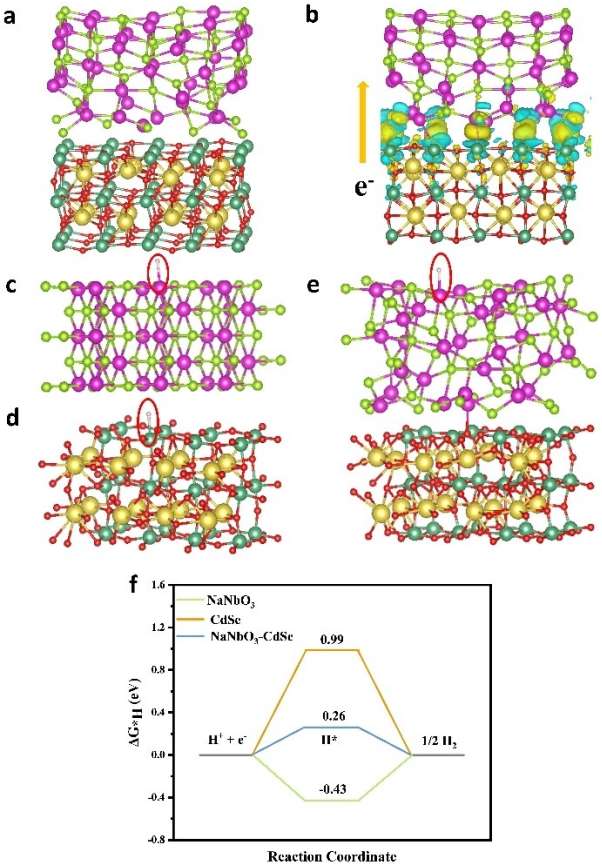

Figure 5. (a) Schematic structure model. (b) Simulated charge density difference of CdSe/$NaNbO_3$. (c-e) Schematic structure models of H adsorption of CdSe, $NaNbO_3$, and CdSe/$NaNbO_3$ heterostructures. (f) Free energy diagrams of reaction of CdSe, $NaNbO_3$ and CdSe/$NaNbO_3$.

electrons from $NaNbO_3$ to CdSe within the composite structure. This observation is consistent with the alterations in binding energy identified in the preceding XPS results. Figure 5c–e displays the schematic structure models of H adsorption of CdSe, $NaNbO_3$, and CdSe/$NaNbO_3$ heterostructures. Furthermore, the H adsorption free energy changes were computed for the $NaNbO_3$, CdSe, and CdSe/$NaNbO_3$ heterostructures, as depicted in Figure 5f. The H-atom adsorption free energy (ΔG_{H^*}) for the CdSe/$NaNbO_3$ composites was determined to be approximately 0.26 eV, displaying proximity to zero relative to CdSe (0.98 eV) and $NaNbO_3$ (−0.43 eV). This finding suggests that the composites exhibit a reduced energy barrier for hydrogen reaction generation, thereby promoting favorable reaction kinetics.

We employed electrostatic potential calculations to derive the work function value for the semiconductor material. As illustrated in Figure 6, significant disparities in the work functions were observed among $NaNbO_3$, CdSe, and the heterostructure. The work function values of $NaNbO_3$, CdSe, and CdSe/$NaNbO_3$ are 3.898 eV, 5.044 eV and 4.379 eV. Notably, the composite work functions fell within an intermediate range, indicating an equilibrium distribution of Fermi level and a consequential shift in the band structure following the composition of the two materials.

Research Article
doi.org/10.1002/cctc.202400502
Chemistry Europe
European Chemical Societies Publishing

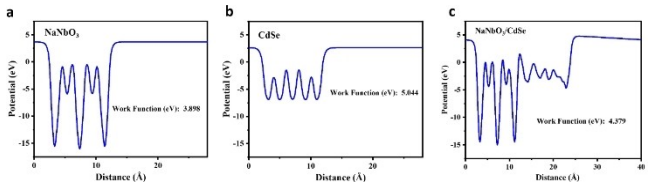

Figure 6. (a-c) Electrostatic potential of $NaNbO_3$, CdSe, and CdSe/ $NaNbO_3$.

Based on the aforementioned characterization analyses, we can approximate the band structure of the two semiconductors.

Prior to their recombination, the conduction band position of $NaNbO_3$ closely resembled that of CdSe. However, due to the wider band gap of $NaNbO_3$, its valence band position exhibited a notable reduction compared to CdSe. Upon the formation of a composite heterojunction, the Fermi energy levels of both materials tend to equilibrate, consequently inducing a shift in the band structures of the two semiconductors. Consequently, we propose the existence of a Z-scheme reaction mechanism in the composite, as demonstrated in Scheme 2. With light excitation, electrons from the valence band of both species are excited to transition to the conduction band. Upon recombination of the two materials, electrons migrate from $NaNbO_3$ to CdSe, exhibiting a tendency to recombine with holes present in the valence band of CdSe, thereby strongly suppressing carrier recombination between the two semiconductors. Subsequently, reduction reactions predominantly occur within the conduction band of CdSe, while oxidation reactions primarily take place within the valence band of $NaNbO_3$. It is worth noting that the photo-generated holes in the CdSe valence band have strong oxidizing properties, which can oxidize Se^{2-}. The combination of electrons transferred from $NaNbO_3$ and holes in CdSe prevents the oxidation of Se^{2-} and enhances the stability of the heterojunction.

Conclusions

In conclusion, we successfully synthesized functional heterostructure composites of CdSe/$NaNbO_3$ to enhance the performance of photocatalytic hydrogen production. The prepared photocatalyst demonstrates excellent photogenerated carrier separation and transfer ability, as well as remarkable stability, owing to the synergistic effect and strong interfacial interaction. The tight interface between $NaNbO_3$ and CdSe effectively suppresses the swift recombination of photoinduced carriers, thereby contributing to improved charge utilization. The CdSe/$NaNbO_3$ heterostructure composites exhibit outstanding photocatalytic hydrogen production performance, achieving a rate of 2510 $\mu mol\, g^{-1} h^{-1}$, which is 5.6 and 2.2 times higher than that CdSe and $NaNbO_3$. Furthermore, the moderate bandgap structure enhances the photo absorption competency of $NaNbO_3$ and mitigates the photocorrosion of CdSe. Additionally, the enhanced light response and efficient carrier migration contribute to further activity enhancement. This straightforward and efficient synthesis method opens up new possibilities for designing high-efficiency photocatalysts for solar energy conversion based on $NaNbO_3$.

Experimental section

Materials

Comprehensive details regarding the materials utilized can be accessed in the *supplementary information* section.

Preparation of $NaNbO_3$ nanorods

The synthesis of $NaNbO_3$ nanorods was accomplished through a two-step hydrothermal and calcination process. Dissolve 1 g of Nb_2O_5 in DI water, then add sodium hydroxide solution (60 mL) at a concentration of 11 M and stir continuously for 1 hour. The mixture

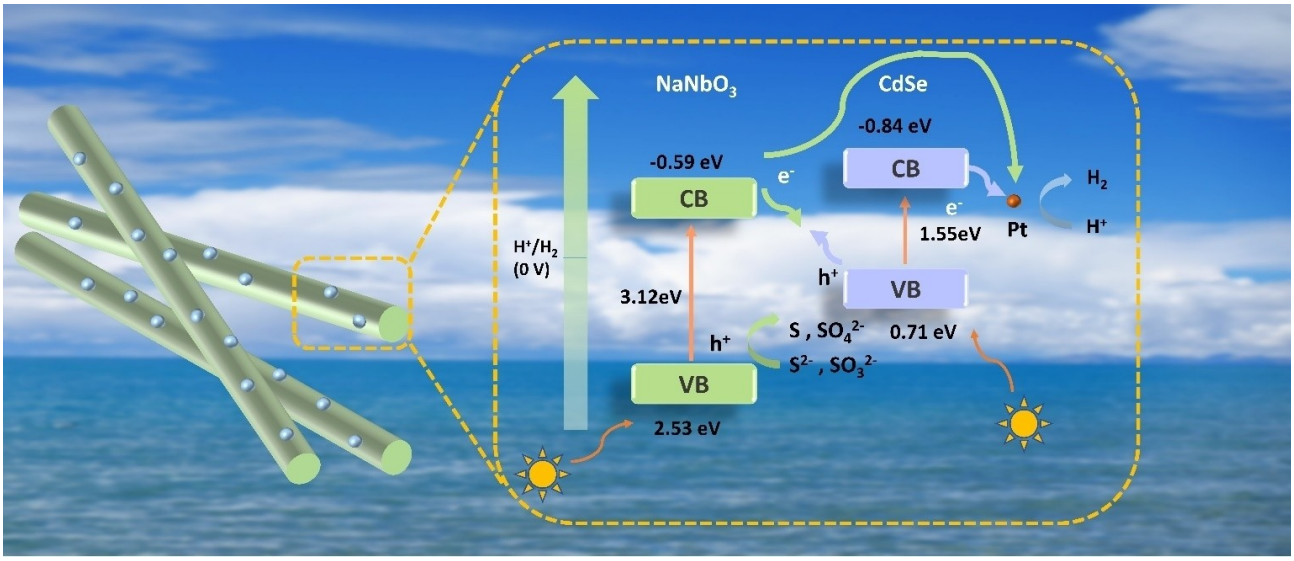

Scheme 2. Illustration of photocatalytic hydrogen evolution mechanism in CdSe/$NaNbO_3$ heterostructure photocatalysis.

was then transferred to a PTFE-lined hydrothermal reactor for 48 hours at 180 °C. After cooling to room temperature, the resulting product was washed to neutral with abundant absolute ethanol and distilled water, followed by vacuum drying at 100 °C for 12 hours. In the N_2 atmosphere, the above reactants will then be calcined at 500 °C for 12 h to finally obtain white $NaNbO_3$ nanorods.

Preparation of CdSe NPs

CdSe NPs were prepared by hydrothermal method. First, while stirring, cadmium chloride hydrate (1.0 mmol), Se powder (1.0 mmol), diethylenetriamine (18 mL), hydrazine hydrate (12 mL) was mixed with DI water, and the above solution was stirred for an additional 1 hour to ensure homogeneous dispersion. The reaction solution was then transferred to a PTFE-lined autoclave and reacted at 100 °C for 12 hours. At the end of the reaction, after being reduced to room temperature, it was washed several times with deionized water and ethanol. The product was freeze-dried overnight to finally get CdSe NPs.

Preparation of CdSe/ $NaNbO_3$

Initially, $NaNbO_3$ (0.29 g) was dispersed in 40 mL of H_2O through sonication. Subsequently, the sodium niobate solution was added into the mixture of cadmium chloride hydrate (1.0 mmol), Se powder (1.0 mmol), diethylenetriamine (18 mL), hydrazine hydrate (12 mL) and DI water. The solution was stirred for an additional 2 h to achieve homogeneous dispersion and then transferred to a PTFE-lined autoclave and reacted at 100°C for 12 h. At the end of the reaction, after being reduced to room temperature, it was washed several times with deionized water and ethanol. The product was freeze-dried overnight to obtain a composite material comprising 40% CdSe/$NaNbO_3$. By altering the mass of sodium niobate added while maintaining a similar procedure, other compositions of xCdSe/$NaNbO_3$ (x = 10, 20, 25, and 30 wt%) were prepared, which were denoted as 10%, 20%, 25%, and 30% CdSe/$NaNbO_3$ composites, respectively.

Characterization

Material characterization, photocatalytic hydrogen evolution strategy, photoelectrochemical tests, and the detailed theoretical calculation method can be found in *supporting information.*

Supporting Information

The authors have cited additional references within the Supporting Information.[45-48]

Acknowledgements

This work was financially supported by the National Key Research and Development Program of China (2021YFA1501404), Natural Science Foundation of Shanghai (22ZR1404200), and Natural Science Foundation of Shanghai Science and Technology Committee (19DZ2270100).

Conflict of Interests

The authors declare that they have no known competing financial interests or personal relationships that could have appeared to influence the work reported in this paper.

Keywords: photocatalytic hydrogen evolution · direct Z-scheme heterostructure · CdSe nanoparticle · $NaNbO_3$ nanorod · strong interfacial interaction

[1] L. Zhang, Y. Cui, F. Yang, Q. Zhang, J. Zhang, M. Cao, W. L. Dai, *J. Mater. Sci. Technol.* **2020**, *45*, 176–186.
[2] L. Zhang, Q. Liu, Y. Chai, F. Yang, M. Cao, W. L. Dai, *J. Phys. Chem. C* **2018**, *122*, 12900–12912.
[3] D. Wei, Y. Tan, Y. Wang, T. Kong, S. Shen, S. S. Mao, *Sci. Bull.* **2020**, *65*, 1389–1395.
[4] L. Sun, Y. Yuan, F. Wang, Y. Zhao, W. Zhan, X. Han, *Nano Energy* **2020**, *74*, 104909.
[5] R. Yousefi, J. Beheshtian, S. M. Seyed-Talebi, H. R. Azimi, F. Jamali-Sheini, *Chem. Asian J.* **2018**, *13*, 194–203.
[6] S. Kumar, N. L. Reddy, H. S. Kushwaha, A. Kumar, M. V. Shankar, K. Bhattacharyya, A. Halder, V. Krishnan, *ChemSusChem* **2017**, *10*, 3588–3603.
[7] S. Kumar, N. L. Reddy, A. Kumar, M. V. Shankar, V. Krishnan, *Int. J. Hydrogen Energy* **2018**, *43*, 3988–4002.
[8] S. Kumar, A. Kumar, V. Navakoteswara Rao, A. Kumar, M. V. Shankar, V. Krishnan, *ACS Appl. Energ. Mater.* **2019**, *2*, 5622–5634.
[9] F. He, Y. Li, *CCS Chem.* **2023**, *5*, 72–94.
[10] X. Zheng, Y. Xue, C. Zhang, Y. Li, *CCS Chem.* **2023**, *5*, 1653–1662.
[11] L. Sun, Y. Zhuang, Y. Yuan, W. Zhan, X. J. Wang, X. Han, Y. Zhao, *Adv. Energy Mater.* **2019**, *9*, 1902839.
[12] F. Yang, Q. Zhang, L. Zhang, M. Cao, Q. Liu, W. L. Dai, *Appl. Catal. B* **2019**, *257*, 117901.
[13] X. Zhang, J. Xiao, M. Hou, Y. Xiang, H. Chen, *Appl. Catal. B* **2018**, *224*, 871–876.
[14] H. Li, H. An, B. Chong, G. Yang, L. Wang, *Chem. Eng. Sci.* **2021**, *238*, 116594.
[15] J. G. Wu, D. Q. Xiao, J. G. Zhu, *Chem. Rev.* **2015**, *115*, 2559–2595.
[16] A. Kumar, M. Kumar, V. Navakoteswara Rao, M. V. Shankar, S. Bhattacharya, V. Krishnan, *J. Mater. Chem. A* **2021**, *9*, 17006–17018.
[17] F. Fresno, P. Jana, P. Reñones, J. M. Coronado, D. P. Serrano, V. A. De La Peña O'Shea, *Photochem. Photobiol. Sci.* **2017**, *16*, 17–23.
[18] M. Stock, S. Dunn, *J. Phys. Chem. C* **2012**, *116*, 20854–20859.
[19] B. H. Xu, B. Z. Lin, Q. Q. Wang, X. T. Pian, O. Zhang, L. M. Fu, *Microporous Mesoporous Mater.* **2012**, *147*, 79–85.
[20] H. Hata, Y. Kobayashi, V. Bojan, W. J. Youngblood, T. E. Mallouk, *Nano Lett.* **2008**, *8*, 794–799.
[21] P. Li, H. Xu, L. Liu, T. Kako, N. Umezawa, H. Abe, J. Ye, *J. Mater. Chem. A* **2014**, *2*, 5606–5609.
[22] Y. A. Zulueta, T. C. Lim, J. A. Dawson, *J. Phys. Chem. C* **2017**, *121*, 23642–23648.
[23] H. Shi, G. Chen, C. Zhang, Z. Zou, *ACS Catal.* **2014**, *4*, 3637–3643.
[24] S. Chen, Y. Hu, L. Ji, X. Jiang, X. Fu, *Appl. Surf. Sci.* **2014**, *292*, 357–366.
[25] H. Guo, X. Liu, C. Bai, Y. Chen, L. Wang, M. Zheng, Q. Dong, D. L. Peng, *ChemSusChem* **2015**, *8*, 486–494.
[26] J. Li, G. Zhan, Y. Yu, L. Zhang, *Nat. Commun.* **2016**, *7*, 11480.
[27] H. Yu, X. Huang, P. Wang, J. Yu, *J. Phys. Chem. C* **2016**, *120*, 3722–3730.
[28] T. P. Hu, Z. Li, L. H. Lu, K. Dai, J. F. Zhang, R. Li, C. H. Liang, *J. Colloid Interface Sci.* **2019**, *555*, 166–173.
[29] Z. Zhang, Y. Y. Kang, L. C. Yin, P. Niu, C. Zhen, R. Z. Chen, X. D. Kang, F. Y. Wu, G. Liu, *J. Mater. Sci. Technol.* **2021**, *95*, 167–171.
[30] D. D. Hou, Y. K. Liu, J. A. Zapien, Y. Y. Shan, S. T. Lee, *Optoelectron. Lett.* **2008**, *4*, 161–164.
[31] S. Wang, B. Y. Guan, X. W. D. Lou, *J. Am. Chem. Soc.* **2018**, *140*, 5037–5040.
[32] J. R. Ran, G. P. Gao, F. T. Li, T. Y. Ma, A. J. Du, S. Z. Qiao, *Nat. Commun.* **2017**, *8*, 13907.
[33] Z. Li, D. Jin, Z. H. Wang, *Int. J. Hydrogen Energy* **2021**, *46*, 6358–6368.
[34] C. Yang, X. Li, M. Li, G. Liang, Z. Jin, *Chin. J. Catal.* **2024**, *56*, 88–103.
[35] T. Yan, R. Ding, D. Ying, Y. Huang, Y. Huang, C. Tan, X. Sun, P. Gao, E. Liu, *J. Mater. Chem. A* **2019**, *7*, 22884–22888.

[36] T. Li, N. Tsubaki, Z. Jin, *J. Mater. Sci. Technol.* **2024**, *169*, 82–104.
[37] P. Li, H. Abe, J. H. Ye, *Int. J. Photoenergy* **2014**, *2014*, 380421.
[38] J. Lv, T. Kako, Z. S. Li, Z. G. Zou, J. H. Ye, *J. Phys. Chem. C* **2010**, *114*, 6157–6162.
[39] P. Gomathisankar, K. Hachisuka, H. Katsumata, T. Suzuki, K. Funasaka, S. Kaneco, *Int. J. Hydrogen Energy* **2013**, *38*, 8625–8630.
[40] S. Chang, H. Gu, H. Zhang, X. Wang, Q. Li, Y. Cui, W.-L. Dai, *J. Colloid Interface Sci.* **2023**, *644*, 304–314.
[41] J. Dong, Y. Shi, C. Huang, Q. Wu, T. Zeng, W. Yao, *Appl. Catal. B* **2019**, *243*, 27–35.
[42] X. Wang, X. Wang, J. Huang, S. Li, A. Meng, Z. Li, *Nat. Commun.* **2021**, *12*, 4112.
[43] S. Saha, G. Das, J. Thote, R. Banerjee, *J. Am. Chem. Soc.* **2014**, *136*, 14845–14851.
[44] Y. Jia, J. Yang, D. Zhao, H. Han, C. Li, *J. Energy Chem.* **2014**, *23*, 420–426.
[45] J. P. Perdew, K. Burke, M. Ernzerhof, *Phys. Rev. Lett.* **1996**, *77*, 3865–3868.
[46] G. Kresse, D. Joubert, *Phys. Rev. B* **1999**, *59*, 1758.
[47] S. Grimme, J. Antony, S. Ehrlich, S. Krieg, *J. Chem. Phys.* **2010** *132*, 154104.
[48] H. J. Monkhorst, J. D. Pack, *Phys. Rev. B* **1976**, *13*, 5188.

Manuscript received: March 13, 2024
Revised manuscript received: April 19, 2024
Accepted manuscript online: April 25, 2024
Version of record online: ■■, ■■

RESEARCH ARTICLE

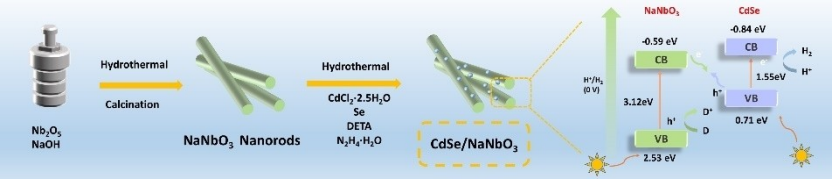

The $CdSe/NaNbO_3$ heterojunctions were fabricated through a hydrothermal approach, facilitating the in-situ growth of CdSe nanoparticles on the surface of $NaNbO_3$ naorods and the heterojunction achieved a photocatalytic hydrogen production of 2510 $\mu mol\, g^{-1}h^{-1}$. The enhancement is contributed to the formation of a Z-scheme heterojunction by the close interface contact between CdSe and $NaNbO_3$.

*L. Gao, S. Chang, H. Gu, H. Zhang, Y. Huang, X. Wang, Q. Li, W.-L. Dai**

1 – 9

Direct Z-Scheme Heterostructure of Nanoparticle-CdSe on Nanorod-$NaNbO_3$: Facile Hydro-thermal Construction and Superior Photocatalytic Activity and Stability in H_2 Evolution